15 micron cutoff HgCdTe Infrared Detector Arrays for Exo-Astronomy

William Forrest[1], Mario S. Cabrera[1], Craig W. McMurtry[1], Meghan L. Dorn[1], and Judith L. Pipher[1]

[1]University of Rochester

November 21, 2022

Abstract

The holy grail of ExoPlanet research is finding and characterizing terrestrial planets orbiting in the habitable zones of a neighboring stars. The first question to be answered is: does the planet have an atmosphere, and what is it's composition. Theory and observation confirm that the one universal atmospheric component should be CO_2. Hence a successful mission must determine it's presence. The most direct path to detection is through the enormously strong 15 micron vibration-rotation feature of CO_2, hence the technology we're developing. Because of the CO_2 in the earth's atmosphere, this requires a space observatory, such as the JWST. Our technology can also be used to detect water vapor and ozone in exoplanet atmospheres, the latter of which indicates abundant life, probably indicative of a 'Cambrian Explosion' event on the exoplanet.

Characterization Results of 15 μm HgCdTe Detector Arrays for Astronomy

The University of Rochester (UR) infrared detector group is working together with Teledyne Imaging Sensors to develop megapixel HgCdTe 15 μm cutoff wavelength detector arrays for future space missions with the goal identifying key components of biosignatures in the atmospheres of exoplanets. This technology could have the capability of identifying the 15 μm CO_2 feature, seen in the three terrestrial planets orbiting in a habitable zone in our solar system. Further investigations of the habitability of such rocky planets would then be determined by the detection of abundant oxygen (from the 9.6 μm ozone feature) and water vapor in their spectra.

To reach the 15 μm cutoff goal, an intermediate step was taken by developing four ~13 μm cutoff wavelength arrays to identify any unforeseen effects related to increasing the cutoff wavelength from the extensively characterized 10 μm cutoff wavelength detector arrays developed for the NEOCam mission. The characterization of the ~13 μm cutoff wavelength HgCdTe arrays at UR allowed us to determine the key dark current mechanisms that limit the performance of these devices at different temperatures and bias when the cutoff wavelength is increased. We present dark current and well depth measurements of three arrays with a 15 μm cutoff wavelength goal (actual cutoffs of 15.2, 15.5, and 16.7 μm at a temperature of 30 K) and a summary of the ~13 μm cutoff arrays.

The goal of this project was to determine if HgCdTe detector arrays are a better option than Si:As detector arrays to cover this wavelength range since HgCdTe devices give very high QE and require significantly less cooling. Si:As devices require cooling down to ~6-8 K, while the best performing ~15 μm HgCdTe device showed a median dark current of 1.4 e^{-}/s (with applied reverse bias of 150 mV, or well depth of 49 ke^{-}) at a temperature of 23 K, while the best ~13 μm device showed a median dark current of 0.2 e^{-}/s with the same applied bias and well depth of 44 ke^{-} but at a temperature of 28 K (Spitzer's focal plane equilibrated to ~28 K after cryogens were exhausted). Although the ~15 μm devices were developed for future space missions, the ~13 μm devices may be used in ground based observatories, giving instruments access to the entire N-band while operating at temperatures attainable with closed cycle coolers, thereby eliminating the need for cryogens.

15 µm Cutoff HgCdTe Infrared Detector Arrays for Exo-Astronomy

William J. Forrest, Mario S. Cabrera, Craig W. McMurtry, Meghan L. Dorn, Judith L. Pipher
University of Rochester, 500 Wilson Blvd., Rochester, NY 14627

I. ABSTRACT

The University of Rochester (UR) infrared detector group is working together with Teledyne Imaging Sensors to develop megapixel HgCdTe 15 µm cutoff wavelength (LW15) detector arrays for future space missions with the goal of identifying key components of biosignatures in the atmospheres of exoplanets. This technology could have the capability of identifying the 15 µm feature, seen in the three terrestrial planets orbiting in a habitable zone in our solar system. Further investigations of the habitability of such rocky planets would then be determined by the detection of abundant oxygen (from the 9.6 µm ozone feature) and water vapor in their spectra.

To reach the 15 µm cutoff goal, an intermediate step was taken by developing ~13 µm cutoff wavelength (LW13) arrays to identify any unforeseen effects related to increasing the cutoff wavelength from the extensively characterized 10 µm cutoff wavelength (LW10) detector arrays developed for the NEOCam mission. The characterization of the LW13 HgCdTe arrays at UR allowed us to determine the key dark current mechanisms that limit the performance of these devices at different temperatures and bias when the cutoff wavelength is increased. We present dark current and well depth measurements of three arrays with a 15 µm cutoff wavelength goal and a summary of the ~13 µm cutoff arrays.

The goal of this project was to determine if HgCdTe detector arrays are a better option than Si:As detector arrays to cover this wavelength range since HgCdTe devices give very high QE and require significantly less cooling. Si:As devices require cooling down to ~6-8 K, while the best performing LW15 HgCdTe device showed a median dark current of 1.4 e^-/s (with applied reverse bias of 150 mV, or well depth of 49 ke^-) at a temperature of 23 K. The best LW13 device showed a median dark current of 0.2 e^-/s with the same applied bias and well depth of 44 ke^- but at a temperature of 28 K (Spitzer's focal plane equilibrated to ~28 K after cryogens were exhausted). Although the LW15 devices were developed for future space missions, the LW13 devices may be used in ground based observatories, giving instruments access to the entire N-band while operating at temperatures attainable with closed cycle coolers, thereby eliminating the need for cryogens.

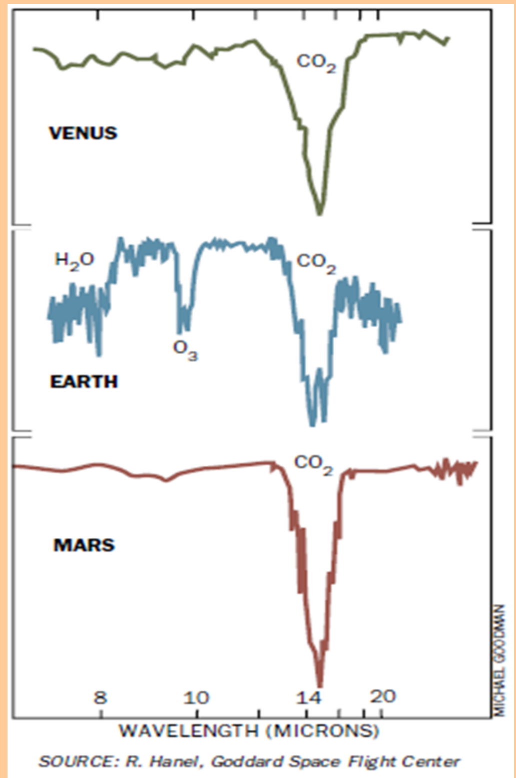

II. THE NEOCAM MISSION

NASA's proposed NEOCam mission requires such arrays for its 6-10 µm band. Working with Teledyne Imaging Sensors (TIS), we have developed such arrays (McMurtry et al. 2013, Girard et al. 2014, Dorn et al. 2016, Bacon et al 2010) implementing HgCdTe photodiodes with the appropriate Hg:Cd ratio. The key performance parameter for these arrays is the dark current, which should be less than the emission from our solar system's zodiacal cloud. For NEOCam the requirement is < 200 e^-/s/pixel for its 18 micron pixels. The QE for these arrays is > 60% before Antireflection coating, and the correlated double sampling read noise is of order 25 e^-. The well-depth requirement is 46 ke^-.

III. ARRAY REQUIREMENTS

In order to passively cool sufficiently in space, the power dissipation of the arrays must be < 1 mW per megapixel. This rules out currently available CTIA readouts, since they utilize active FETs in each unit cell. The power requirement is well within the performance of source-follower-per-detector readouts such as the Hawaii 1RG and 2RG used with the WISE, HST and JWST missions. Low-power readouts, such as the H1RG, have a source-follower amplifier FET in each pixel's 'unit cell'. The unit cell FETs need be active (drawing current) only during the reading of the unit cell's voltage. Typically only one or a few FETs are drawing current at a time, leading to the low power dissipation quoted above.

Bailey et al. (1998) and Bacon et al.(2010) showed that the dominant dark current mechanism at low temperatures for LWIR HgCdTe photodiodes is quantum mechanical tunneling. In contrast to 'thermal' dark current from 'diffusion' and 'generation-recombination' (see McMurtry et al. 2013), tunneling is highly bias voltage dependent. It is the great challenge of LWIR HgCdTe arrays to produce photodiodes with sufficiently small tunneling dark currents with hundreds of mV of back-bias. Because of the exponential dependence of tunneling probability, this challenge becomes dramatically stiffer for cutoff wavelengths exceeding the 10 µm requirement of NEOCam. Hence the first step in our development program at TIS to produce 15 µm cutoff wavelength arrays was to produce 13 µm cutoff arrays.

IV. 13 µm DEVICES

TIS grew nine wafers, from which we selected the six best with 24 grade A/B megapixel die, and successfully hybridized four H1RG arrays for further testing at UR. The cutoff wavelength is measured at 30 K, and decreases by about 0.25 µm for a 10 K temperature increase. Typical QEs shortward of the cutoff are about 70%, which is quite good since approximately 22-25% of incident light is reflected at the back surface. Typical read noises are below 25 e^- at 30 K (McMurtry et al. 2013, Cabrera et al. 2019).

H1RG-18367 and H1RG-18508 have the same standard structure as the 10 µm NEOCam arrays, only extrapolated to 13 µm, while H1RG-18369 and H1RG-18509 were designed to mitigate quantum tunneling dark currents. The QE and cutoff wavelength measurements in Table 1 were provided by TIS. Figure 1 shows the QE and cutoff wavelength measured at UR with a temperature of 30 K and an applied bias of 250 mV. Within measurement uncertainties, the QE and cutoff wavelength measured at UR confirmed the measurements provided by TIS.

Detector H1RG-	Wafer	Cutoff Wavelength (µm)	QE (6-10 µm)
18367	3757	12.8	74%
18508	3755	12.7	73%
18369	3763	12.4	72%
18509	3759	12.6	73%

Table 1: Cutoff wavelength and QE for all four LW13 arrays measured at a temperature of 30 K. QE values are expected to increase if arrays had anti-reflecting coating.

A. Application to Ground Based Astronomy

With cutoff wavelengths of at least 13.5 µm, the whole 'N band', running from just short of 8 to just beyond 13 µm, will be available. The current devices show high QE and low dark currents to provide good performance in ground-based cameras and spectrometers. Since the detectors are photo-diodes, the performance should be excellent under these conditions. The great strength of this technology, compared to the commonly used Si:As BIB arrays, is the high temperature of operation. Sufficiently low dark current is achieved at circa 30 K, a temperature easily reachable by commercially available closed-cycle coolers. These only require electrical power at the mountaintops where observatories are built, much preferable to the stored cryogens commonly used.

The Hawaii mux used here would not be appropriate for a ground based array. The low well depth and the leisurely readout would be problematic. A different type of multiplexer is indicated, probably based on the CTIA structure. These devices use feedback to maintain a constant detector bias as the signal is accumulated. The reason for rejecting them for our space based observatories, i.e. high power dissipation, is not an issue at a ground based observatory — electricity is cheap there and cryo-coolers would be adequate.

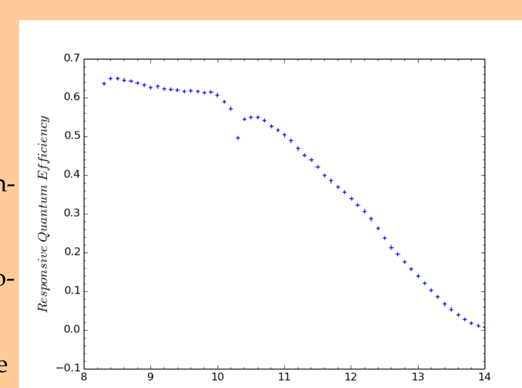

Figure 1: Cutoff wavelength and QE measured at UR for H1RG-18369. at a temperature of 30 K and 250 mV of applied bias.

B. Operability: Dark Current and Well Depth

The key detector parameters that limit the performance of these arrays is the dark current and well depth, and therefore determine the pixel operability. Though operability requirements depend on specific applications of these devices, similar operability requirements in dark current and well depth as those for the NEOCam mission are used as a benchmark to compare the performance of the different arrays at different temperatures and applied bias to determine the best pixel design that will be pursued when increasing the cutoff wavelength to 15 µm. Our imposed operability requirements include dark currents < 200 e^-/s, and well depth greater than ~40 ke^- for an applied bias of 150 mV. At a temperature of 28 K and 150 mV of applied bias, all four LW13 devices have operabilities > 90%, where three of the four devices had a median dark current < 1 e^-/s with similar distribution to that shown in Figure 2 for H1RG-18508. The fourth array, H1RG-18367, had a median ``dark'' current of ~10 e^-/s due to a glow from the unit cell FETs of the multiplexer. Operable pixels in these devices corresponds to those below and to the right of the dashed lines in Fig. 2 and 3.

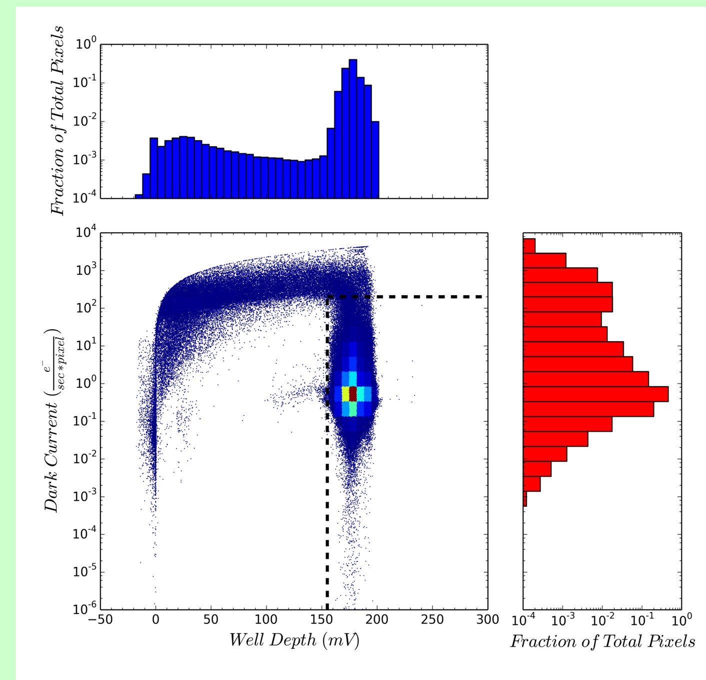

Figure 2: Current in the dark *vs.* well depth distribution per pixel for H1RG-18508 at a temperature of 28 K and an applied bias of 150 mV. Dashed horizontal and vertical lines correspond to the operability requirements for dark current (< 200 e^-/s) and well depth (>155 mV, ~40ke^-) respectively.

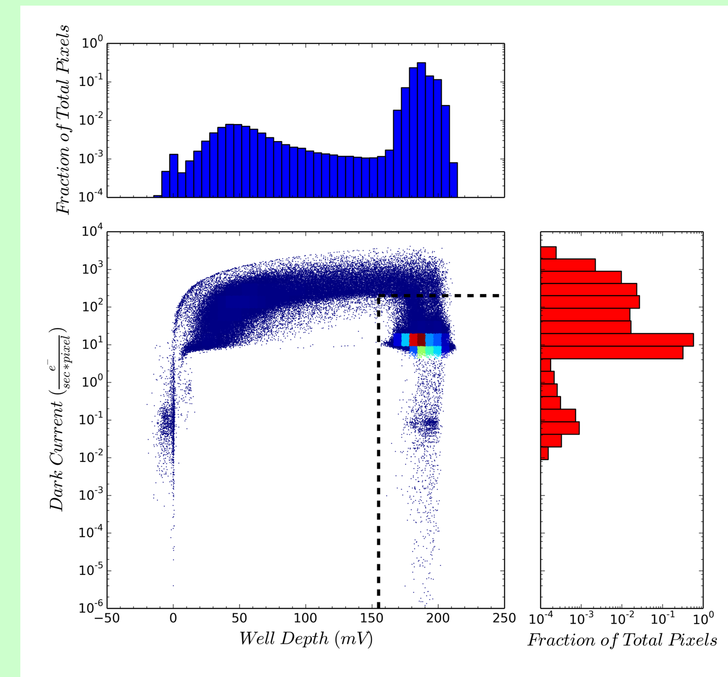

Figure 3: Current in the dark *vs.* well depth distribution per pixel for H1RG-18367 at a temperature of 28 K and an applied bias of 150 mV. Dashed horizontal and vertical lines correspond to the operability requirements for dark current (< 200 e^-/s) and well depth (>155 mV, ~40ke^-) respectively.

Inoperability criteria for these detectors consists of low well-depth (<155 mV, about 40 ke^-) and high dark current (>200 e^-/s). At 28 K and 150 mV of applied bias, low well-depth was the main source of inoperability in pixels for all four arrays as shown in the Venn diagrams below. The inadequate well-depth of the pixels to the left of the dotted line in the operability plots results from pixel debiasing before the first sample. We employ the 'reset-read-read-…' sampling method. The first 'read' is delayed by up to 5.5 sec from the reset, thus a high dark current pixel can become debiased. The implied initial dark current, > 8,000 e^-/s, would disqualify that pixel in any case.

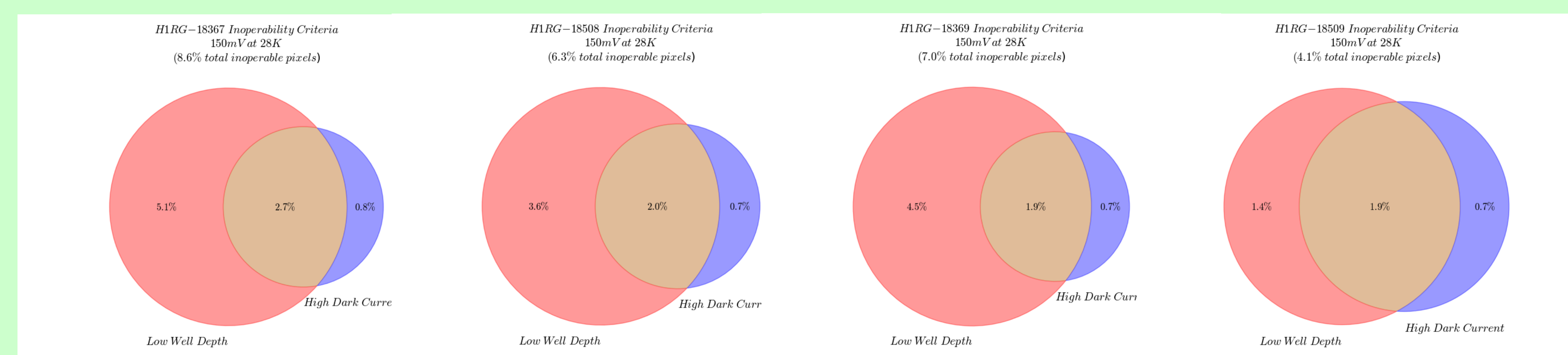

Figure 4: Venn diagrams showing the criteria for inoperable pixels in all four LW13 devices at a temperature of 28 K and 150 mV of applied bias.

When the inoperable pixels at low applied bias are mapped (Fig. 5), all four arrays at this temperature and bias showed a prominent cross-hatching pattern in three distinct directions that have been identified to lie parallel to the intersection of the {111} slip planes in zinc blende crystals and the growth plane of these arrays, forming misfit dislocations along these three particular directions. This cross-hatching pattern is an imprint of the crystal axes of the CdZnTe substrate upon which our HgCdTe layers were grown. The FFT of the operability map (upper left corner in Fig. 5) shows the three distinct directions of the cross-hatching pattern (rotated by 90 degrees) very clearly.

The very large dark currents that result in low well depths among inoperable pixels are due to trap-assisted quantum mechanical tunneling, a result of the misfit dislocations that propagate to the p-n junction of a pixel along the cross-hatching pattern (Bailey et al. 1998).

The vertical cross-hatching pattern is responsible for the horizontal line in the FFT power spectrum. The cross-hatching pattern, is seen in some of the LW10 devices (less predominately) grown for NEOCam by TIS and in all of the LW15 devices as well.

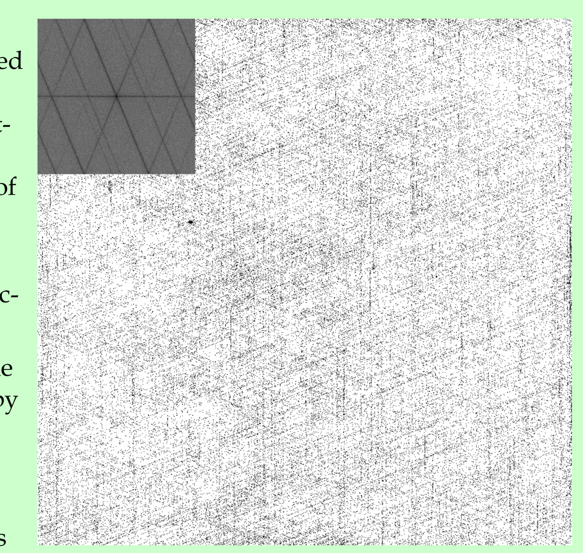

Figure 5: Operability map for H1RG-18367 at a temperature of 28 K and 150 mV of applied reverse bias. Inoperable pixels are shown in black. >90% of pixels are deemed operable.

B. Dark Current Model

At large applied bias (350 mV), only H1RG-18509 had operabilities > 90%, while the other three devices had operabilities ~0% due to very large dark currents. The three arrays with near 0% operability at large applied reverse bias exhibited a strong bias dependent dark current as shown for a pixel in H1RG-18508 in Fig. 6, where the initial dark current increased from 0.4 e^-/s with 150 mV of applied bias to 788 e^-/s. with 350 mV of applied bias. Similarly, H1RG-18367 and H1RG-18369 had dark currents exceeding the 200 e^-/s operability requirement with 350 mV of applied bias. H1RG-18509 (array with experimental design to mitigate tunneling currents) had a median dark current of 1.8 e^-/s with 350 mV of applied bias. To show the dark current mechanisms present in these arrays as a function of bias and temperature, dark current models were fitted to data. We showed that the array design of H1RG-18509 successfully mitigated the affects of band-to-band tunneling dark current, responsible for the inoperability of the other three devices at large biases. Band-to-band tunneling dark currents affect all pixels uniformly.

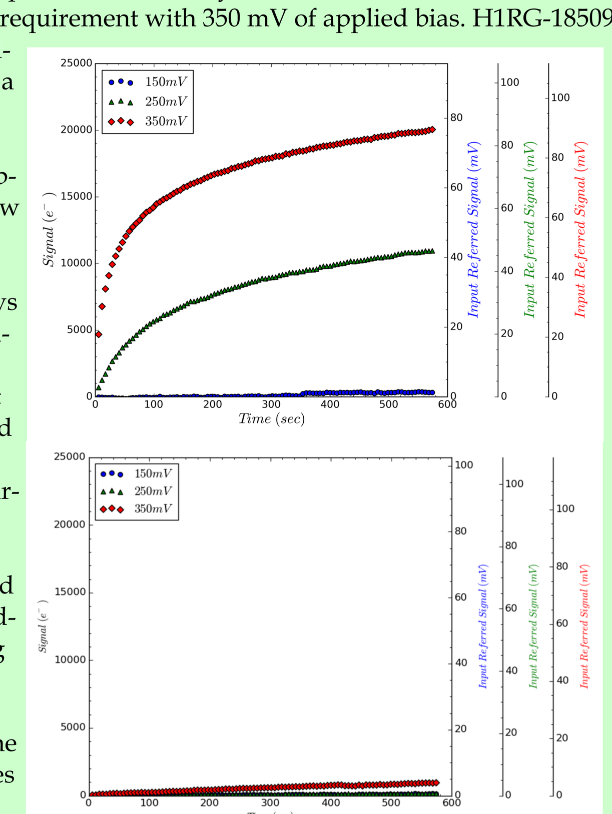

Figure 6: Dark discharge history of a typical operable (at low biases) pixel in (top) H1RG-18508 and (bottom) H1RG-18509 at a temperature of 28K and three different applied biases. The different axes on the right result from the decrease in capacitance as applied bias increases.

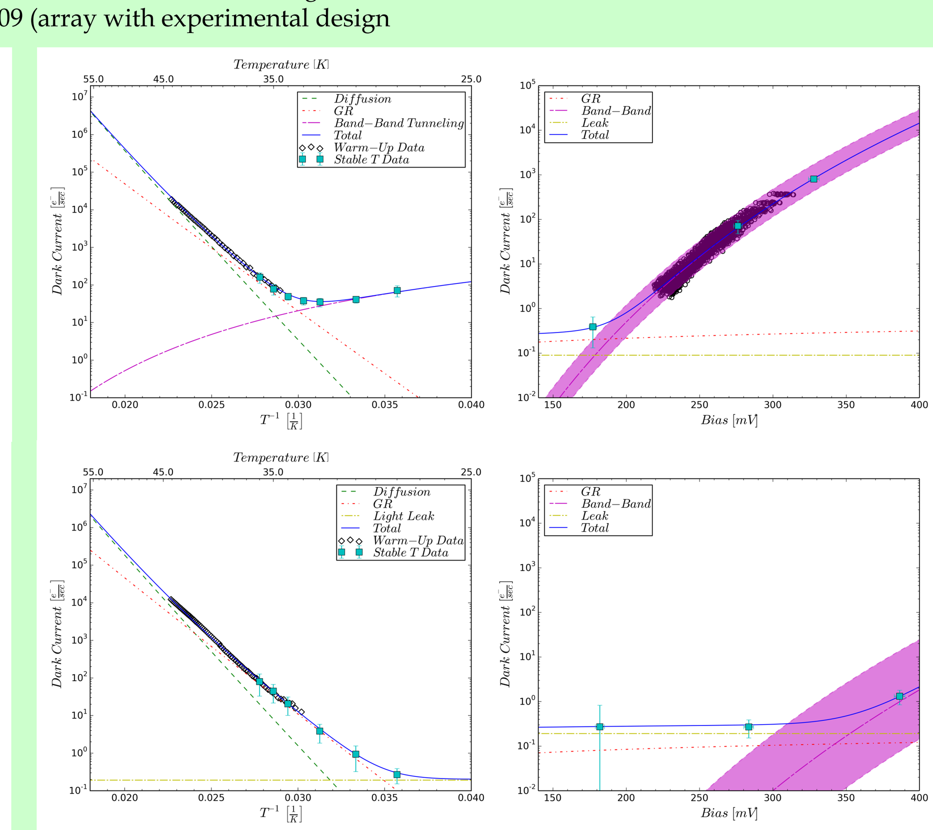

Figure 7: Mean dark current as a function of temperature (150mV of bias) and bias (28K) for (top) 36 randomly selected operable pixels in H1RG-18508 and (bottom) 50 pixels in H1RG-18509. Individual I-V curves for the 36 pixels in H1RG-18508 are plotted to show the band-to-band tunneling behavior. The shaded region corresponds to the ± 1 standard deviation away from the mean of the band-to-band tunneling model fitted to ~12,000 operable pixels.

V. 15 µm DEVICES

The UR infrared detector group received three 1024x1024 pixel LW15 detector arrays bonded to H1RG multiplexers for the final phase of this project from TIS. Table 2 includes the quantum efficiency (QE) and cutoff wavelength measurements provided by TIS for the three LW15 arrays at a temperature of 30 K from the PECs that were grown and processed at the same time as the megapixel arrays.

The design of LW13 device H1RG-18509 was selected as the best structure to move forward with the production of 15 µm cutoff wavelength detector arrays. The analysis of the three LW15 arrays showed an improvement in the diode structure to reduce tunneling currents further. For H1RG-20303, at a temperature of 23 K and an applied bias of 350 mV, the measured dark current (see Fig. 9 (b)) is approximately two orders of magnitude smaller than was expected from an array with the same performance as H1RG-18509, only with the cutoff wavelength extended to match that of H1RG-20303.

Detector H1RG-	Wafer	Cutoff Wavelength (µm)	QE (6-12 µm)
20302	3995	16.7	81%
20303	3994	15.5	83%
20304	4018	15.2	80%

Table 2: Cutoff wavelength and QE for all three LW15 arrays measured and provided by TIS at a temperature of 30 K. QE values are expected to increase if arrays had anti-reflecting coating. These QE measurements are above the theoretical value (78%), but are within experimental measurement error.

The longer cutoff wavelength of these LW15 devices leads to larger dark currents if operated at similar temperatures and biases as the LW13 devices. Figure 8 shows the median dark current *vs.* temperature for all LW13 and LW15 devices with an applied bias of 150 mV. The LW15 devices show dark currents ~ 2-3 orders of magnitude higher than the LW13 devices at a temperature of 28 K. Although the LW15 devices would require to be operated at lower temperatures to achieve comparable dark currents to the LW13 devices, the shortest wavelength LW15 device had a median dark current below 100 e^-/s at 28 K. These results are very encouraging since the thermal dark current in LW15 devices at these temperature appears to be dominated by G-R dark currents which depend on trap sites in the depletion region. With further improvement on the processing method of these arrays, the dark current may continue to improve for future devices.

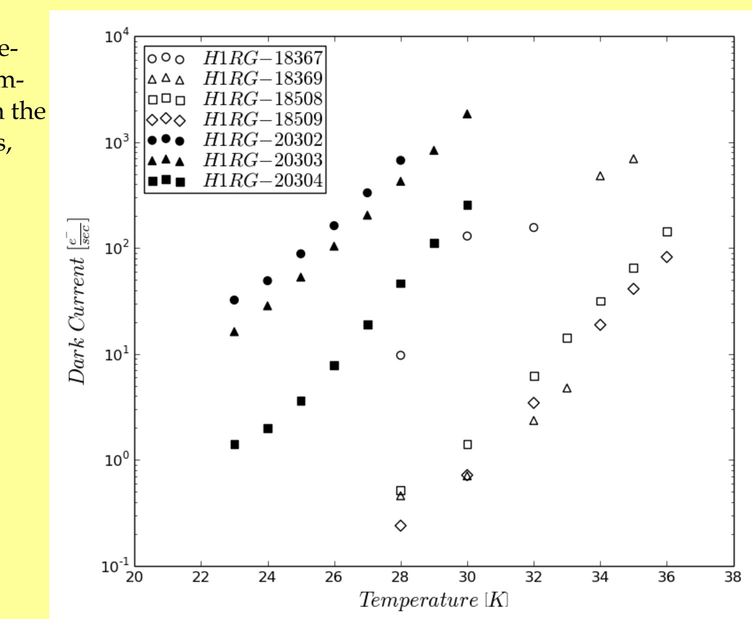

Figure 8: Median dark current *vs.* temperature for all LW13 and LW15 devices with an applied bias of 150 mV. The solid data points correspond to the LW15 arrays. A multiplexer glow affected and increased all dark current measurements for H1RG-18367 and at temperatures > 33K for H1RG-18369.

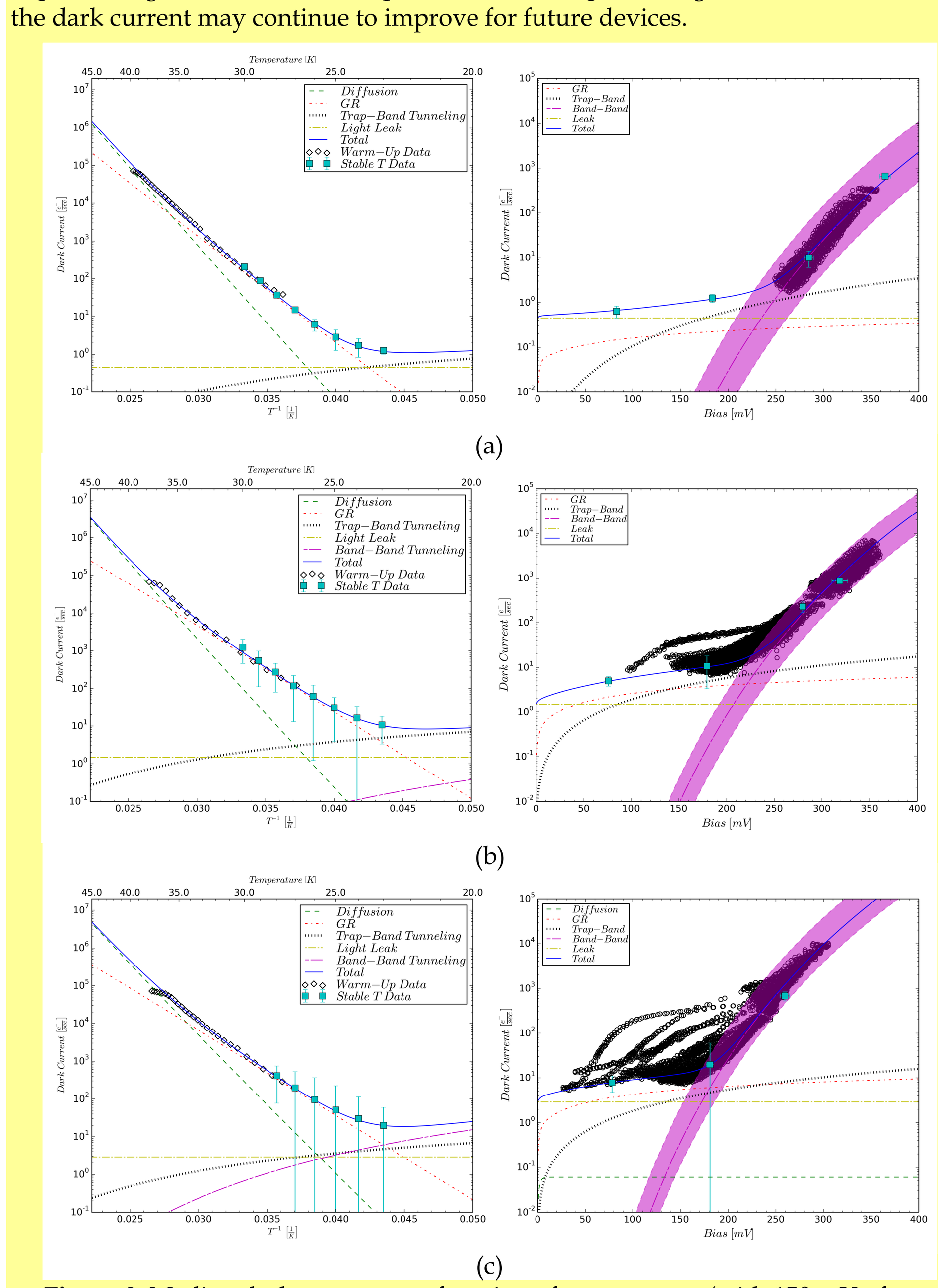

Figure 9: Median dark current as a function of temperature (with 150 mV of applied bias) and bias (at a temperature of 23 K) for 36 randomly selected operable pixels in (a) H1RG-20304, (b) H1RG-20303, and (c) H1RG-20302.

Many of the features observed in the devices for the first phase of this project were seen in these devices. At low applied biases and low temperatures, pixels with very large dark currents or low well depth lied along the same cross-hatching pattern shown in Fig. 5. Among well behaved pixels (at low bias), similarly to the LW13 devices, the dark current is dominated by band-to-band tunneling at larger applied biases. Figure 9 shows the dark current data as a function of temperature and bias for the three LW15 devices. These devices showed an increase in trap-to-band tunneling over the LW13 devices among well behaved pixels at low biases. Several pixels exhibited bias dependent trap-assisted dark currents, where certain traps contribute to the dark current only at biases larger than a given threshold voltage for those traps.

The dark currents results for these devices are very encouraging since at large biases we were able to show that band-to-band tunneling is the dominant component of dark current. Further improvement in the device design by TIS would continue to decrease this component of dark current. Furthermore, as was mentioned earlier, advancement in the processing method would decrease trap-to-band tunneling and G-R currents which dominate the dark current at low biases.

VI. Conclusions

For the first phase of the project, at 28K and 150 mV, more than 90% of the pixels in all four LW13 megapixel arrays showed dark currents <200 e^-/s, and well depths of at least 37 ke^-. It was shown that larger applied biases (> 200 mV) will result in an exponentially increasing dark current for three of the four devices, where the median dark currents for these three devices were between 379-780 e^-/s at a temperature of 28 K and an applied bias of 350 mV. This increasing dark current is due to band-to-band tunneling dark currents, affecting the majority of pixels uniformly. The successful experimental design of array H1RG-18509 mitigated these tunneling currents, with a median dark current and well depth of 1.8 e^-/s and 81 ke^- respectively at a temperature of 28 K and an applied bias of 350 mV.

The second phase of this project showed the successful and improved array design to further mitigate band-to-band tunneling dark currents at longer cutoff wavelengths. Array H1RG-20304 has a cutoff wavelength closest to the goal of this project and was the best performing of the three devices for this phase, where at a temperature of 28 K and an applied bias of 250 mV, 80% of the pixels have dark currents below 200 e^-/s and well depths greater than 54 ke^- (median dark current and well depth of 58 e^-/s and 67 ke^- respectively). The future use of this technology in space missions is very promising, where the characterization of these devices has demonstrated the ability of this technology to operate at temperatures that can be attained through passive cooling in space.

References

- Cabrera, M.S., et al., ``Characterization of a 15 µm Cutoff HgCdTe Detector Array for Astronomy", Journal of Astronomical Telescopes, Instruments, and Systems (**In Press**).
- Cabrera, M. S., et al., ``Development of 13 µm Cutoff HgCdTe Detector Arrays for Astronomy," Journal of Astronomical Telescopes, Instruments, and Systems **5**(3), 1 - 18 - 18 (2019).
- Girard, J. J., et al., "Cosmic ray response of megapixel LWIR arrays from TIS", Proceedings of the SPIE, Volume 9154, id. 91542A 10 pp. (2014).
- Bailey, R. B., et al., "Prospects for large-format IR astronomy FPAs using MBE-grown HgCdTe detectors with cutoff wavelength > 4 µm", Proc. SPIE Vol. 3354, p. 77-86. (1998).
- Bacon, C. M., "Development of Long Wave Infrared Detectors for Space Astronomy", PhD Thesis, University of Rochester, Rochester, NY. (2006)
- Bacon, C. M., et al., "Effect of dislocations on dark current in LWIR HgCdTe photodiodes", Proc. SPIE Vol. 7742. (2010)
- Dorn, M. et al., "Proton irradiation results for long-wave HgCdTe infrared detector arrays for NEOCam", Journal of Astronomical Telescopes and Instrumentation 2(3), 036002. (2016)
- McMurtry, C. W., Lee D., Beletic J., et al., "Development of sensitive long-wave infrared detector
- arrays for passively cooled space missions," Opt. Eng., **52(9)**, 1-10. (2013)
- McMurtry, C. W., et al., "Candidate 10 micron HgCdTe Arrays for the NEOCam Space Mission", Proc. SPIE 9915, 99150D. (2016)

Acknowledgements

William Forrest and the Rochester group acknowledge support by NASA grant NNX14AD32GS07